Kinetic temperatures for a granular mixture

Steven R. Dahl and Christine M. Hrenya
Department of Chemical Engineering, University of Colorado, Boulder, Colorado 80309

Vicente Garzó
Departamento de Física, Universidad de Extremadura, E-06071 Badajoz, Spain

James W. Dufty
Department of Physics, University of Florida, Gainesville, Florida 32611
(Received 21 May 2002; published 30 September 2002; published 1 October 2002)

An isolated mixture of smooth, inelastic hard spheres supports a homogeneous cooling state with different kinetic temperatures for each species. This phenomenon is explored here by molecular dynamics simulation of a two component fluid, with comparison to predictions of the Enskog kinetic theory. The ratio of kinetic temperatures is studied for two values of the restitution coefficient $\alpha=0.95$ and 0.80, as a function of mass ratio, size ratio, composition, and density. Good agreement between theory and simulation is found for the lower densities and higher restitution coefficient; significant disagreement is observed otherwise. The phenomenon of different temperatures is also discussed for driven systems, as occurs in recent experiments. Differences between the freely cooling state and driven steady states are illustrated.

DOI: 10.1103/PhysRevE.66.041301 PACS number(s): 45.70.Mg, 05.20.Dd, 51.10.+y, 47.50.+d

I. INTRODUCTION

The dissipative nature of granular media is captured by an idealized fluid of smooth, inelastic hard spheres. When isolated and homogenized such a system rapidly approaches a homogeneous cooling state (HCS) for which all time dependence of the distribution function occurs through the temperature. The latter, defined in the usual way via the average kinetic energy, decays in time (''cooling'') due to the inelastic collisions. The existence of the HCS and associated cooling rate is well established for a one-component system by theory [1], Monte Carlo simulation [2], and molecular dynamics simulation [3]. Recently, it has been shown from the Enskog kinetic theory that a mixture of inelastic hard spheres also has a HCS under the same conditions [4]. The condition that all time dependence occurs through the temperature requires that the cooling rates for the kinetic temperatures for each species must be the same. It follows directly that the kinetic temperatures are different for mechanically different species, reflecting a violation of the equipartition theorem valid for elastic collisions. A prediction for the ratio of temperatures in a binary mixture as a function of mass ratio, size ratio, composition, density, and restitution coefficients was obtained from an approximate solution to the Enskog equations. The accuracy of this approximate result has been recently confirmed by Monte Carlo simulation of the Enskog equations [5].

The objective here is to demonstrate the phenomenon of a HCS and two temperatures in a broader context by molecular dynamics (MD) simulation for a binary mixture of inelastic hard spheres. MD simulation avoids any assumptions inherent in the kinetic theory or approximations made in solving the kinetic equations. It is shown here that MD simulation supports the existence of a HCS for mixtures with different kinetic temperatures for each species but with a common cooling rate. The dependence of the temperature ratio on mechanical properties and state conditions is found to be in good agreement with predictions of the Enskog kinetic theory, except at high density and strong dissipation. In the latter case, significant quantitative deviations from the Enskog theory are observed but the concept of a HCS and two temperatures is preserved [6].

The HCS can be given a time independent representation by transformation to suitable dimensionless variables [7,8]. In this form, it is similar to the steady state obtained for *homogeneously driven* granular fluids. The latter are obtained by adding stochastic sources to the kinetic equation or MD dynamics to do work on the system that compensates for the collisional cooling. The resulting homogeneous steady state is qualitatively the same as the dimensionless HCS, but the quantitative differences are expected to make it closer to *locally driven* steady states observed in experiments on vibrated granular media. Studies of driven states have been extended to mixtures both theoretically [9] and experimentally [10,11]. The comparisons of the temperature ratio for the HCS mixture and that for the two types of homogeneously driven mixtures are given below. Their relationship to a locally driven system is also discussed.

The plan of the paper is as follows. In Sec. II, we show that the Liouville equation for a binary granular mixture supports a scaling solution describing the HCS. A transformation to dimensionless variables allows to get the (constant) temperature ratio $\gamma=T_1(t)/T_2(t)$ in terms of the parameters of the mixture. An approximate evaluation of the temperature ratio can be made from the Enskog kinetic theory, as is shown in Sec. III. In Sec. IV, the Enskog predictions are compared with those obtained from MD simulations. Such a comparison shows a quite good agreement for the lower densities considered, but significant discrepancies between the theory and the simulation appear for high density and strong dissipation. The existence of two temperatures in driven granular mixtures [9,12,13] and its possible connection with

recent experiments is analyzed in Sec. V. Finally, the paper ends in Sec. VI with a brief discussion on the relevance of the results presented here.

II. HOMOGENEOUS COOLING STATE FOR A MIXTURE

The system considered is a binary mixture of N_1 and N_2 smooth hard spheres of masses m_1 and m_2, and diameters σ_1 and σ_2. In general, collisions among all pairs are inelastic and are characterized by three constant restitution coefficients α_{ij}, which can be different for the three types of pair collisions. The state of the system at time t is specified by the $N=N_1+N_2$ particle phase space density $\rho(\Gamma,t)$, which is a solution to the Liouville equation [14]. In all of the following, attention is restricted to spatially homogeneous states. In this section, it is further assumed that the system is isolated. The properties of primary interest are the overall temperature $T(t)$ associated with the total kinetic energy, and the partial temperatures $T_i(t)$ associated with the kinetic energies of each species. They are defined as

$$T(t)=\sum_{i=1}^{2} x_i T_i(t), \quad \frac{3}{2}N_i T_i(t)=\left\langle \sum_{\mu=1}^{N_i} \frac{1}{2} m_i v_\mu^2; t \right\rangle. \tag{1}$$

The brackets denote a phase space average over the state of the system at time t and $x_i=N_i/N$ is the composition. The time dependence of $T(t)$ and $T_i(t)$ follows from the Liouville equation that gives [4,14,15]

$$T^{-1}\partial_t T=-\zeta, \quad T_i^{-1}\partial_t T_i=-\zeta_i, \tag{2}$$

where ζ_i is the cooling rate associated with the partial temperature T_i and ζ is the total cooling rate. They are given by

$$\zeta=\frac{1}{T}\sum_{i=1}^{2} x_i T_i \zeta_i, \tag{3}$$

$$\zeta_i=-\frac{m_i}{3n_i T_i}\sum_{j=1}^{2}\int d\mathbf{v}_1 v_1^2 \int d\mathbf{v}_2 \int d\mathbf{r}_{12}\overline{T}_{ij}(\mathbf{r}_{12},\mathbf{v}_1,\mathbf{v}_2) f_{ij}^{(2)}(\mathbf{r}_{12},\mathbf{v}_1,\mathbf{v}_2,t). \tag{4}$$

Here, n_i is the number density of species i, $\mathbf{r}_{12}$ is the relative position of the two particles, and $f_{ij}^{(2)}(\mathbf{r}_{12},\mathbf{v}_1,\mathbf{v}_2,t)$ are the reduced two-particle distribution functions for a particle of type i and one of type j, obtained from $\rho(\Gamma,t)$ by integrating over degrees of freedom for all other particles. The binary collision operators are defined by [14,15]

$$\overline{T}_{ij}(\mathbf{v}_1,\mathbf{v}_2,\mathbf{r}_{12})=\sigma_{ij}^2\int d\hat{\boldsymbol{\sigma}}\ \Theta(\hat{\boldsymbol{\sigma}}\cdot\mathbf{g}_{12})(\hat{\boldsymbol{\sigma}}\cdot\mathbf{g}_{12})[\alpha_{ij}^{-2}\delta(\mathbf{r}_{12}-\boldsymbol{\sigma})b_{ij}^{-1}-\delta(\mathbf{r}_{12}+\boldsymbol{\sigma})], \tag{5}$$

where $\sigma_{ij}=(\sigma_i+\sigma_j)/2$, $\hat{\boldsymbol{\sigma}}$ is a unit vector directed along the line of centers from the sphere of species i to that of species j at contact, Θ is the Heaviside step function, and $\mathbf{g}_{12}=\mathbf{v}_1-\mathbf{v}_2$. Also, b_{ij}^{-1} is a substituting operator, $b_{ij}^{-1}F(\mathbf{g}_{12})=F(b_{ij}^{-1}\mathbf{g}_{12})$, which changes any function of $\mathbf{v}_1$ and $\mathbf{v}_2$ to the same function of the restituting velocities $\mathbf{v}_1'$ and $\mathbf{v}_2'$:

$$\mathbf{v}_1'=\mathbf{v}_1-\mu_{ji}(1+\alpha_{ij}^{-1})(\hat{\boldsymbol{\sigma}}\cdot\mathbf{g}_{12})\hat{\boldsymbol{\sigma}},$$

$$\mathbf{v}_2'=\mathbf{v}_2+\mu_{ij}(1+\alpha_{ij}^{-1})(\hat{\boldsymbol{\sigma}}\cdot\mathbf{g}_{12})\hat{\boldsymbol{\sigma}}, \tag{6}$$

where $\mu_{ij}=m_i/(m_i+m_j)$. Upon writing Eqs. (4) and (5) we have taken into account that for an homogeneous system the spatial dependence of f_{ij} occurs only through $\mathbf{r}_{12}$.

In general, all three temperatures and associated cooling rates will be different and depend on the initial preparation. The time evolution of the ratio of the two partial temperatures $\gamma(t)=T_1(t)/T_2(t)$ follows from the second equality of Eq. (2):

$$\partial_t \ln\gamma=\zeta_2-\zeta_1. \tag{7}$$

For a system with elastic collisions, $\rho(\Gamma,t)$ rapidly approaches to the Gibbs distribution with a single constant temperature. This requires $\zeta_1=\zeta_2$, and $T_i\propto T$ in the Gibbs state. The form of the velocity distribution functions and the constancy of the temperature then gives $T_1=T_2=T$ and $\zeta_1=\zeta_2=0$. This equality of the temperatures is the equipartition theorem for classical statistical mechanics. The vanishing of the cooling rates is a consequence of the system approaching towards a steady state.

If the collisions are inelastic, the system still approaches rapidly a special state known as the HCS. As with the Gibbs state, the velocities scale with the temperature for a dimensionless universal distribution of the form

$$\rho_{\mathrm{HCS}}(\Gamma,t)=[\ell v(t)]^{-3N}\rho_{\mathrm{HCS}}^*(\{\mathbf{r}_{ij}^*,\mathbf{v}_i^*\}). \tag{8}$$

Here $\mathbf{r}_{ij}^*=\mathbf{r}_{ij}/\ell$ denotes the dimensionless relative coordinate for particles i and j, and ℓ is some appropriate characteristic length scale such as the mean free path. The dimensionless velocities $\mathbf{v}_i^*=\mathbf{v}_i/v_0(t)$ are scaled relative to the thermal velocity defined by $v_0(t)=\sqrt{2T(t)(m_1+m_2)/m_1m_2}$. This scaling has the same consequences as described above for elastic collisions: $T_i(t)$

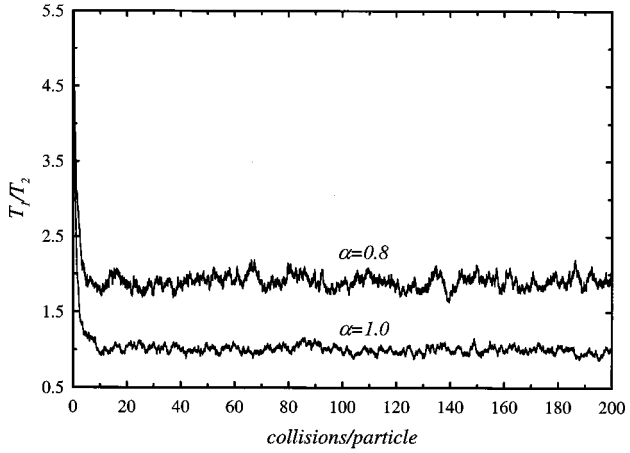

FIG. 1. Time evolution of $\gamma(t)=T_1(t)/T_2(t)$ for $\phi=0.1$, $\sigma_1/\sigma_2=\phi_1/\phi_2=1$, $m_1/m_2=8$, and two values of α: $\alpha=0.8$ and $\alpha=1$.

$\propto T(t)$, $\gamma(t)\to$const, and so $\zeta_1=\zeta_2$. However, Eq. (8) is not a steady state since the cooling rates ζ_i do not vanish. Also, the form of $\rho^*_{\rm HCS}$ is not the same as for the Gibbs state so there is no *a priori* reason to expect that the temperatures should be equal [4]. In fact, as indicated below, they are equal only in the limit of mechanically equivalent particles or elastic collisions.

The simplest test of the evolution towards a HCS with the assumed velocity scaling is the approach of $\gamma(t)$ to a constant value. This is illustrated in Fig. 1 from MD simulation using 1000 particles of the same size and composition, but with the mass ratio $m_1/m_2=8$. The total solid volume fraction is $\phi=0.1$ and all coefficients of restitution are equal. Here, $\phi=\phi_1+\phi_2$, where

$$\phi_i=\frac{1}{6}\pi n_i\sigma_i^3 \tag{9}$$

is the species volume fraction of the component i. We consider two values of the restitution coefficient: $\alpha=0.8$ and $\alpha=1$. We observe that in the elastic case ($\alpha=1$) the mixture approaches the Gibbs state with the temperature ratio $\gamma(t)\to 1$, as expected from equipartition. In the inelastic case ($\alpha=0.8$), $\gamma(t)$ approaches a constant value ($\gamma\simeq 2$ with fluctuations less than 5%) after about 10 collisions per particle. It is seen that the HCS for inelastic collisions is approached on the same time scale as the Gibbs state for elastic collisions. Further details of the MD simulation are discussed below.

III. ENSKOG KINETIC THEORY

The kinetic temperatures defined by Eq. (1) can be given in an equivalent form in terms of the one-particle reduced distribution function $f_i^{(1)}(\mathbf{v},t)$ as

$$T_i(t)=\frac{1}{3}\frac{m_i}{n_i}\int d\mathbf{v}\, v^2 f_i^{(1)}(\mathbf{v},t). \tag{10}$$

The one-particle reduced distribution function $f_i^{(1)}(\mathbf{v},t)$ obeys the exact first Bogoliubov-Born-Green-Kirkwood-Yvon (BBGKY) hierarchy equations

$$\partial_t f_i^{(1)}(\mathbf{v}_1,t)=\sum_{j=1}^{2}\int d\mathbf{v}_2\int d\mathbf{r}_{12}\overline{T}_{ij}(\mathbf{r}_{12},\mathbf{v}_1,\mathbf{v}_2)f_{ij}^{(2)}(\mathbf{r}_{12},\mathbf{v}_1,\mathbf{v}_2,t). \tag{11}$$

To be more specific about the dependence of the temperatures on the parameters of the mixture, it is sufficient to specify the reduced distribution functions $f_{ij}^{(2)}(\mathbf{r}_{12},\mathbf{v}_1,\mathbf{v}_2,t)$ in Eq. (11). This also determines the cooling rates from Eq. (4). These distribution functions occur only in the combination $\overline{T}_{ij}f_{ij}^{(2)}$, so knowledge of $f_{ij}^{(2)}$ is required only for pairs of particles at contact and only on the precollision hemisphere. A practical approximation for these conditions is obtained by neglecting velocity correlations and expressing the two-particle distribution functions in terms of the single-particle distribution functions,

$$f_{ij}^{(2)}(\mathbf{r}_{12},\mathbf{v}_1,\mathbf{v}_2,t)\to f_i^{(1)}(\mathbf{v}_1,t)f_j^{(1)}(\mathbf{v}_2,t)\chi_{ij}(\mathbf{r}_{12},t). \tag{12}$$

The single-particle distributions are independent of position since only homogeneous states are considered here. The spatial correlation function $\chi_{ij}(\mathbf{r}_{12},t)$ is evaluated at contact and its choice is given below. The one-particle distribution functions can be determined by using this same approximation in the exact first BBGKY hierarchy equations, which becomes

$$\partial_t f_i^{(1)}(\mathbf{v}_1,t)=\sum_{j=1}^{2} J_{ij}[\mathbf{v}_1|f_i^{(1)}(t),f_j^{(1)}(t)], \tag{13}$$

where $J_{ij}[f_i^{(1)},f_j^{(1)}]$ is the Enskog collision operator [14]. These are now closed equations for $f_i^{(1)}$ and constitute the Enskog kinetic theory for the granular binary mixture.

For the HCS the scaling form (8) implies a similar scaling form for $f_i^{(1)}(\mathbf{v}_1,t)$,

$$f_i^{(1)}(\mathbf{v},t)=n_i v_0^{-3}(t)f_i^*(v^*). \tag{14}$$

Furthermore, $\chi_{ij}(\mathbf{r}_{12}=\sigma_{ij},t)\to\chi_{ij}\equiv$const since all time dependence occurs through the velocity scaling. For practical purposes, and to agree with the equilibrium limit for elastic collisions, χ_{ij} is taken to be the equilibrium pair correlation function. A good approximation is given by the Carnahan-Starling form [16]

$$\chi_{ij}=\frac{1}{1-\phi}+\frac{3}{2}\frac{\xi}{(1-\phi)^2}\frac{\sigma_i\sigma_j}{\sigma_{ij}}+\frac{1}{2}\frac{\xi^2}{(1-\phi)^3}\left(\frac{\sigma_i\sigma_j}{\sigma_{ij}}\right)^2, \tag{15}$$

where $\xi=\pi(n_1\sigma_1^2+n_2\sigma_2^2)/6$. Comparison with computer simulations for binary molecular hard sphere mixtures have shown that the Carnahan-Starling equation (15) is accurate in most of the fluid region, although it fails for high densities and for large diameter ratios [17]. Given the values considered in our simulations, we expect that the approximation (15) turns out to be quite accurate to evaluate the pair correlation function χ_{ij}. In terms of the reduced distributions f_i^*, the Enskog kinetic equations become

$$\frac{\zeta_i^*}{2}\frac{\partial}{\partial \mathbf{v}^*}\cdot(\mathbf{v}^* f_i^*)=\sum_{j=1}^{2} J_{ij}^*[\mathbf{v}^*|f_i^*,f_j^*], \tag{16}$$

where $\zeta_i^*=\zeta_i/n v_0\sigma_{12}^2$ and $J_{ij}^*=(v_0^2/nn_i\sigma_{12}^2)J_{ij}$ are given, respectively, by

$$\zeta_i^*[f_i^*,f_j^*]=-\frac{2}{3}\lambda_i\sum_{j=1}^{2}\int d\mathbf{v}_1^* v_1^{*2} J_{ij}^*[f_i^*,f_j^*], \tag{17}$$

$$J_{ij}^*[v_1^*|f_i^*,f_j^*]=x_j\chi_{ij}\left(\frac{\sigma_{ij}}{\sigma_{12}}\right)^2\int d\mathbf{v}_2^*\int d\hat{\boldsymbol{\sigma}}\ \Theta(\hat{\boldsymbol{\sigma}}\cdot\mathbf{g}_{12}^*)$$
$$\times(\hat{\boldsymbol{\sigma}}\cdot\mathbf{g}_{12}^*)[\alpha_{ij}^{-2}f_i^*(v_1'^*)f_j^*(v_2'^*)$$
$$-f_i^*(v_1^*)f_j^*(v_2^*)], \tag{18}$$

where $\mathbf{g}_{12}^*=\mathbf{g}_{12}/v_0$, $\lambda_i=(v_0/v_{0i})^2=T/(T_i\mu_{ji})$, with $j\neq i$, is the square of the ratio of the thermal velocity to that for species i, and $v_{0i}=\sqrt{2T_i/m_i}$.

In the dimensionless form (16) the Enskog equations are time independent. The pair of coupled equations (16) must be solved self-consistently with the expressions for the cooling rates in Eq. (4) to determine f_i^* and $\zeta_1^*=\zeta_2^*=\zeta^*$. The temperature $T(t)$ is then obtained from the known cooling rate by solving the first of Eqs. (2), and the distribution functions $f_i^{(1)}(\mathbf{v},t)$ are fully determined. The kinetic temperature for each species is obtained from Eq. (16) as

$$T_i(t)=T(t)\frac{2}{3}\mu_{ji}^{-1}\int d\mathbf{v}^* v^{*2} f_i^*(v^*). \tag{19}$$

As anticipated, $T_i(t)\propto T(t)$ in the HCS and $\gamma=T_1/T_2$ becomes

$$\gamma=\frac{\mu_{12}}{\mu_{21}}\frac{\int d\mathbf{v}^* v^{*2} f_1^*(v^*)}{\int d\mathbf{v}^* v^{*2} f_2^*(v^*)}. \tag{20}$$

This is essentially the approach used in the numerical Monte Carlo solution [5] to the Enskog equation.

In practice, only approximate solutions for the HCS are possible (an exception is a recent exact result for a one-dimensional Maxwell model [18]) and a different approach is followed. First, the solution is represented as a series in velocity polynomials, with the leading terms given by

$$f_i^*(v^*)\to\left(\frac{\lambda_i}{\pi}\right)^{3/2}e^{-\lambda_i v^{*2}}\left[1+\frac{c_i}{4}\left(\lambda_i^2 v^{*4}-5\lambda_i v^{*2}+\frac{15}{4}\right)\right]. \tag{21}$$

Thus, the weight function (Gaussian) for each species is chosen to be scaled relative to the thermal velocity for that species, introducing explicitly the unknown species temperatures. The coefficients c_i measure the deviation of f_i^* from the chosen reference Gaussians. The cooling rates are now calculated as explicit functions of λ_i and c_i from Eq. (17). With these known, the Enskog equations can be solved to determine c_i as functions of λ_i by substitution of Eq. (21) into the Enskog equations, taking the v^4 moment of those equations, and retaining terms up through linear in c_i. Finally, the λ_i are determined from the consistency condition for the HCS, $\zeta_1^*=\zeta_2^*$. The detailed results for c_i and λ_i as functions of the fluid parameters are given in Refs. [4] and [5] and will not be repeated here.

IV. COMPARISON OF THEORY AND SIMULATION

The approximation (21) provides detailed predictions for the species temperatures as functions of the mass ratio, size ratio, composition, density, and restitution coefficients. The quality of this approximate solution to the Enskog equations has been recently confirmed by direct Monte Carlo simulation of those equations over a wide range of the parameter space [5]. Specifically, the parameter space over which the solution (21) has been verified is the mass ratio m_1/m_2, the concentration ratio n_1/n_2, the ratio of diameters σ_1/σ_2, the reduced density $n\sigma_{12}^3$, and the (common) restitution coefficient $\alpha\equiv\alpha_{11}=\alpha_{22}=\alpha_{12}$. However, uncertainties remain regarding the accuracy of the Enskog equations themselves. An appropriate means to study the concept of the HCS and the associated different partial temperatures, as well as to study the domain of validity of the Enskog kinetic theory is via MD simulations. Since the parameter space here is quite large the tests of the theory and concepts are quite stringent.

Two different values of the solid volume fractions ϕ have been considered here, $\phi=0.1$ and $\phi=0.2$, both representing a moderately dense fluid. All coefficients of restitution were set equal and two values considered, $\alpha=0.8$ and $\alpha=0.95$, both representing moderately strong dissipation. The temperature ratio γ in the HCS has been studied for three cases in each state. In the first case (case I) γ is determined as a function of the mass ratio m_1/m_2 for $\sigma_1/\sigma_2=\phi_1/\phi_2=1$. The second case (case II) determines γ as a function of size ratio σ_1/σ_2 for $m_1/m_2=\phi_1/\phi_2=1$, while the third case (case III) determines γ as a function of composition ϕ_1/ϕ_2 for $m_1/m_2=8$ and $\sigma_1/\sigma_2=2$.

The granular system under consideration does not contain external force fields, and thus the particles travel in straight-line trajectories between collisions. Correspondingly, an event-driven algorithm is employed in the MD simulations. The simulated particles are modeled as inelastic, frictionless

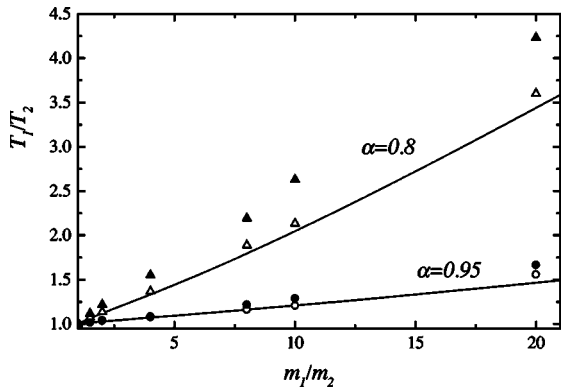

FIG. 2. Plot of the temperature ratio T_1/T_2 as a function of the mass ratio m_1/m_2 for $\sigma_1/\sigma_2=\phi_1/\phi_2=1$, and two different values of α: $\alpha=0.95$ (solid line and circles) and $\alpha=0.8$ (solid line and triangles). The lines are the Enskog predictions and the symbols refer to the MD simulation results. The open (solid) symbols correspond to $\phi=0.1$ ($\phi=0.2$).

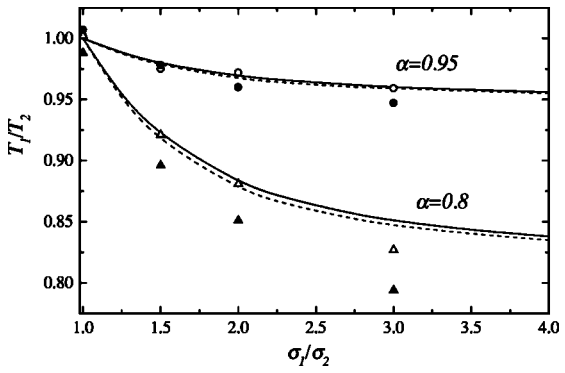

FIG. 3. Plot of the temperature ratio T_1/T_2 as a function of the size ratio σ_1/σ_2 for $m_1/m_2=\phi_1/\phi_2=1$, and two different values of α: $\alpha=0.95$ (lines and circles) and $\alpha=0.8$ (lines and triangles). The lines are the Enskog predictions and the symbols refer to the MD simulation results. The solid (dashed) lines correspond to $\phi=0.1$ ($\phi=0.2$), while the open (solid) symbols correspond to $\phi=0.1$ ($\phi=0.2$).

hard spheres (i.e., collisions are both binary and instantaneous) moving in a three-dimensional space with standard periodic boundaries. The initial particle velocities are uniformly distributed about a zero mean, regardless of the particle size. These velocities are then adjusted to ensure that the net system momentum is zero.

As indicated in Fig. 1, the system reaches a steady value for the temperature ratio γ within 10 collisions per particle for a wide class of initial conditions. However, it is known that the HCS is unstable to long wavelength perturbations so that spontaneous deviations from the HCS occur at long times. To assure that γ is measured in the HCS, the temperature $T(t)$ is monitored as a function of time to determine if the predicted cooling from the scaling form (8) (Haff's law) is maintained [19]. In order to keep the computational time reasonable for each of the simulations (about 1 h), the total number of particles was kept constant at $N=1000$ for all simulations. Data from the first 10 collisions per particle (or 10 000 total collisions) were used to determine the slope of $T(t)$. Specifically, the $\ln[T(t)/T(0)]$ was sampled 1000 times during this initial portion of the simulation. Somewhat surprisingly, a smooth linear decrease in $\ln[T(t)/T(0)]$ was observed throughout the 1000 samples, and a linear regression analysis was employed to evaluate the slope of the Haff's law plot. Following evaluation of the slope of $\ln[T(t)/T(0)]$, collection of the $\gamma=T_1(t)/T_2(t)$ data commenced. This data collection period involved as many as 200 additional collisions per particle (or 200 000 total collisions) including 50 000 equally spaced measurements of γ. The phrase ''as many as'' refers to the fact that the data collection would cease (with fewer than 50 000 measurements of the energy ratio) if the measured value of $\ln[T(t)/T(0)]$ deviated from the expected value of $\ln[T(t)/T(0)]$ by more than 5%. Violation of the Haff's law restriction occurred frequently when the mass ratio m_1/m_2 was greater than 4. Additionally, simulations of equal mass particles ($m_1/m_2=1$) violated the Haff's law restriction when $\alpha=0.8$ and $\phi=0.2$.

Figure 2 shows the results for case I, γ as a function of mass ratio. The symbols represent the simulation data where the circles are for $\alpha=0.95$ and the triangles are for $\alpha=0.8$. In addition, open (solid) symbols correspond to $\phi=0.1$ ($\phi=0.2$). The simulation values reported represent the average from three identical simulations, with a standard deviation typically less than 3%. The Enskog prediction of the preceding section is given by the solid lines (the theory does not predict any dependence on ϕ in this case). The agreement between the theory and the simulation is seen to be quite good at $\alpha=0.95$, over the whole range of mass ratios. The agreement is also quite good at $\alpha=0.8$ and $\phi=0.1$. However, systematic deviations from the Enskog theory for large mass ratios are obtained in the simulations at $\phi=0.2$.

Figure 3 shows the results for case II, γ as a function of size ratio. The notation is the same as in Fig. 2, where now the solid line refers to $\phi=0.1$ while the dashed line is for $\phi=0.2$. The agreement for both $\alpha=0.95$ and $\alpha=0.8$ is quite good at $\phi=0.1$, except for the largest size ratio at $\alpha=0.8$. The density dependence of the theory is weaker than that from the simulation, and large differences are observed at $\phi=0.2$.

Figure 4 shows the results for case III, γ as a function of composition. We observe that both the theory and the simulation predict a very weak influence of composition on the temperature ratio. In addition, the trends are similar to those of Figs. 2 and 3. Good agreement is obtained for $\alpha=0.95$ at both $\phi=0.1$ and $\phi=0.2$. At stronger dissipation there is a strong density dependence in the simulation that is not reproduced by the theory.

V. DRIVEN SYSTEMS AND EXPERIMENTS

The existence and details of different temperatures for each species in a HCS is now well established by kinetic theory and simulation. The related experiments [10,11] and simulations [12,13] on driven steady states also show different temperatures, but the detailed dependence on the control parameters appears to be different. The driven steady states are achieved from external forces that do work at the same rate as collisional cooling. In the experiments this is accom-

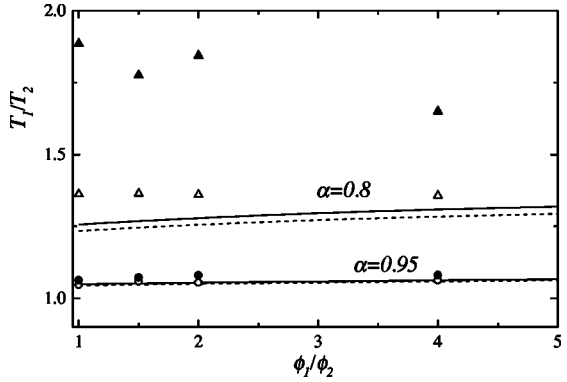

FIG. 4. Plot of the temperature ratio T_1/T_2 as a function of composition ϕ_1/ϕ_2 for $m_1/m_2=8$, $\sigma_1/w\sigma_2=2$, and two different values of α: $\alpha=0.95$ (lines and circles) and $\alpha=0.8$ (lines and triangles). The lines are the Enskog predictions and the symbols refer to the MD simulation results. The solid (dashed) lines correspond to $\phi=0.1$ ($\phi=0.2$), while the open (solid) symbols correspond to $\phi=0.1$ ($\phi=0.2$).

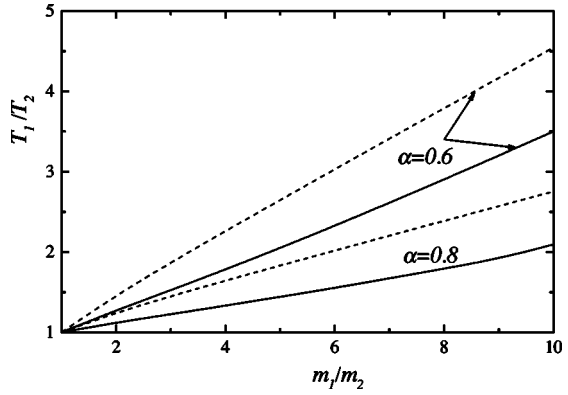

FIG. 5. Plot of the temperature ratio T_1/T_2 as a function of the mass ratio m_1/m_2 for $\phi=0$, $\sigma_1/\sigma_2=\phi_1/\phi_2=1$, and two different values of α: $\alpha=0.8$ and $\alpha=0.6$. The solid lines are the results for the HCS, while the dashed lines are the results for the driven steady state achieved from the stochastic thermostat.

plished by vibrating the system so that it is locally driven at the walls. Far from these walls a steady state is studied whose properties are presumed to be insensitive to the details of the driving forces. The velocities of the particles can be measured using high speed photography [10] or positron emission particle tracking [11]. The objective of this section is to explore similarities and differences between the temperature ratios for a binary mixture in the HCS and in a driven steady state.

As a first analysis, a *homogeneously* driven steady state is considered. This does not correspond directly to any experimental driving source, but has been considered extensively as a representation of driven systems for the one-component fluid [20]. In this case a uniform external nonconservative force, frequently referred to as a ''thermostat,'' is applied to compensate for collisional cooling. Two types of thermostats are considered here. One is a deterministic Gaussian thermostat widely used in nonequilibrium molecular dynamics simulation for the molecular fluids [21]. The force is similar to a Stokes law drag force, linear in the velocity, but with the opposite sign so that it heats rather than cools the system. The ''friction'' constant can be chosen to exactly compensate for the collisional cooling. At the level of kinetic theory, the introduction of such an external force leads to a steady state equation that is *identical* to Eq. (16). It is easily confirmed that the same is true at the level of the Liouville equation in the appropriate dimensionless variables. Thus, there is an exact correspondence between the HCS and this type of driven steady state and, in particular, the dependence of γ on the control parameters is the same.

A second method of driving the system homogeneously is by means of a stochastic Langevin force representing Gaussian white noise [22]. This force for each species is written as $\mathcal{F}_i=m_i\boldsymbol{\xi}_i$, where the covariance of the stochastic acceleration is

$$\langle \xi_{i\alpha}(t)\xi_{j\beta}(t')\rangle = 2D\delta_{ij}\delta_{\alpha\beta}\delta(t-t'). \tag{22}$$

Note that the covariance for the random accelerations is taken to be the same for each species [9,23]. This force induces a diffusion in the velocity space, with diffusion coefficient D. At the level of kinetic theory this leads to an additional source represented by a Fokker-Planck collision operator, in addition to the Enskog collision operator. The steady state Enskog equations then take the form

$$0=\sum_j J_{ij}[\mathbf{v}|f_i^{(1)},f_j^{(1)}]+D\left(\frac{\partial}{\partial v}\right)^2 f_i^{(1)}. \tag{23}$$

Multiplying by $m_i v_i^2/2$ and integrating gives the relationship of D to the cooling rates ζ_i, i.e., $D=\zeta_i T_i/2m_i$. This in turn implies the steady state condition

$$\zeta_1\frac{T_1}{m_1}=\zeta_2\frac{T_2}{m_2}. \tag{24}$$

The cooling rates are no longer equal, as for the HCS, and the dependence of the temperatures on the control parameters will be different as well.

The procedure for determining the temperatures for the stochastically driven steady state is the same as that described in Sec. III. The steady state distribution is represented as an expansion of the form (21) and the coefficients are now determined from moments of the set (23). The cooling rates are then determined from this solution using Eq. (17), and the condition (24) gives an equation for the temperature ratio γ. Figures 5, 6, and 7 illustrate the differences between the HCS and the stochastic steady state for $\alpha=0.6$ and 0.8. The solid lines are the results for the HCS, while the dashed lines are the results for the driven steady state. The dependence of γ on mass ratio is shown in Fig. 5 for $\phi=0$ and $\phi_1/\phi_2=\sigma_1/\sigma_2=1$. This dependence is seen to be considerably stronger in the driven state. The dependence on composition is shown in Fig. 6 for $\phi=0$, $m_1/m_2=2$, and $\sigma_1/\sigma_2=1$. Finally, the dependence on overall packing fraction ϕ is shown in Fig. 7 for $\phi_1/\phi_2=1$ and $m_1/m_2=\sigma_1/\sigma_2=2$. In this last case, the effect of increased density is greater for the HCS than for the driven steady state.

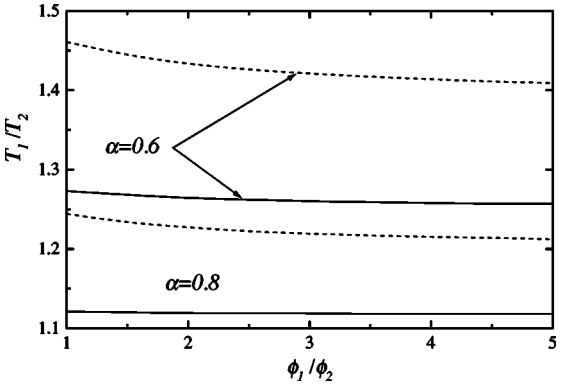

FIG. 6. Plot of the temperature ratio T_1/T_2 as a function of composition ϕ_1/ϕ_2 for $\phi=0$, $m_1/m_2=2$, $\sigma_1/\sigma_2=1$, and two different values of α: $\alpha=0.8$ and $\alpha=0.6$. The solid lines are the results for the HCS, while the dashed lines are the results for the driven steady state achieved from the stochastic thermostat.

The HCS and homogeneously driven steady states are seen to be qualitatively similar, with only quantitative differences. It remains to understand their relationship to locally driven wall forces. An example is described for the Boltzmann equation in the Appendix. There the boundary condition is a sawtooth vibration of one wall such that every particle encountering the wall has a reflected speed increased by twice the velocity of the wall in the component normal to the wall. The steady state condition is considerably more complex than for the HCS or the homogeneously driven steady states. In the limit that the wall velocity is large compared to the thermal velocities of each species, the condition (24) is recovered. This suggests that the results obtained from this condition are plausible first approximations for qualitative comparisons with experimental results [9]. However, the detailed nature of the driven state requires further characterization before quantitative conclusions can be drawn. This is suggested by the study of a driven state in the absence of gravity [24] where the system is found to be well described by hydrodynamics away from the wall, but the steady state is strongly inhomogeneous.

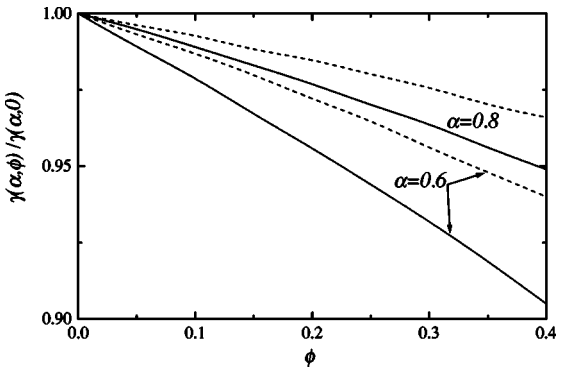

FIG. 7. Plot of the relative temperature ratio $\gamma(\alpha,\phi)/\gamma(\alpha,0)$ as a function of the total solid volume fraction ϕ for $m_1/m_2=\sigma_1/\sigma_2=2$, $\phi_1/\phi_2=1$, and two different values of α: $\alpha=0.8$ and $\alpha=0.6$. The solid lines are the results for the HCS, while the dashed lines are the results for the driven steady state achieved from the stochastic thermostat.

VI. DISCUSSION

The primary results of this study are twofold. First, the MD simulations confirm the rapid approach to a HCS with two kinetic temperatures determined by a common cooling rate. This occurs over a wide range of densities, composition, and mass and size ratios, for both moderate and strong dissipation. The second result is confirmation of the Enskog kinetic theory to provide a quantitative description of this phenomenon for the lower densities and weaker dissipation cases. This includes densities well outside the Boltzmann limit and applies throughout the parameter space of mechanical properties. The analysis here is a test of the Enskog prediction for the cooling rates, which are essentially transport properties (collision rates). The good agreement obtained is further testimony to the utility of this remarkable equation for fluids with elastic and inelastic collisions, including mixtures.

The failure of the Enskog theory at high densities is expected from experience with normal fluids. This is due to multiparticle collisions, including recollision events (ring collisions). The latter are expected to be stronger for fluids with inelastic collisions where the colliding pairs tend to become more focused. It appears that the range of densities for which the Enskog description applies decreases with increasing dissipation. This is the case observed here and also elsewhere for the self-diffusion coefficient [8]. The specific mechanism responsible for the large discrepancies at high densities and its quantitative prediction remains an open problem.

The magnitude of the difference between the two kinetic temperatures generally increases as the mechanical differences increase, although the dependence on volume fraction is weak. Also, there is a significant dependence on the inelasticity and total volume fraction. The experiments in Ref. [10] show a similar strong dependence on mass ratio, but no significant dependence on inelasticity, total density, or composition. The detailed correspondence between the simple model homogeneous states considered here and the locally driven states of experiments needs refinement, although generally the same trends are observed [9].

The hydrodynamics for binary mixtures of inelastic hard spheres has been derived recently, including the effects of two kinetic temperatures [25]. Although only the overall temperature associated with both species serves as a hydrodynamic field, the transport coefficients depend on the temperature ratio γ. Since the latter is a function of the composition and density, there are additional contributions to the transport coefficients. Differences as large as 50% are found for some coefficients.

ACKNOWLEDGMENTS

S.R.D. is grateful for the support provided by the National Science Foundation Graduate Program. V.G. acknowledges partial support from the Ministerio de Ciencia y Tecnología (Spain) through Grant No. BFM2001-0718.

APPENDIX: LOCAL BOUNDARY CONDITIONS

The Enskog equations with boundary conditions can be written as [26]

$$(\partial_t+\mathbf{v}_1\cdot\boldsymbol{\nabla}-T_{Wi})f_i^{(1)}(\mathbf{r},\mathbf{v}_1;t)=\sum_j J_{ij}[\mathbf{v}_1|f_i^{(1)}(t),f_j^{(1)}(t)]. \tag{A1}$$

Here, T_{Wi} describes interactions of particles of type i with the boundaries

$$T_{Wi}f_i^{(1)}(\mathbf{r},\mathbf{v}_1;t)=\int_\Xi d\mathbf{s}\,\delta(\mathbf{r}-\mathbf{s}) \times\left\{\int d\mathbf{v}'P(\mathbf{v}_1,\mathbf{v}')|\hat{\mathbf{n}}\cdot\mathbf{v}'|f_i^{(1)}(\mathbf{r},\mathbf{v}';t) -\Theta(-\hat{\mathbf{n}}\cdot\mathbf{v}_1)|\hat{\mathbf{n}}\cdot\mathbf{v}_1|f_i^{(1)}(\mathbf{r},\mathbf{v}_1;t)\right\}. \tag{A2}$$

This is similar to the usual Boltzmann collision operator with the first term representing a gain in the population of particles with velocity $\mathbf{v}_1$ due to collisions with the wall, and the second term representing a corresponding loss. The probability density for a velocity $\mathbf{v}_1$ after the collision with the wall, given an incident velocity $\mathbf{v}'$ has the form

$$P(\mathbf{v}_1,\mathbf{v}')=\Theta(\hat{\mathbf{n}}\cdot\mathbf{v}_1)K(\mathbf{v}_1,\mathbf{v}')\Theta(-\hat{\mathbf{n}}\cdot\mathbf{v}'). \tag{A3}$$

The two Θ functions characterize the incident particles as directed toward the wall and the reflected particle directed away from the wall, where the normal $\hat{\mathbf{n}}$ is directed toward the interior of the system. The kernel $K(\mathbf{v}',\mathbf{v}_1)$ characterizes the change in the half space velocity distributions at the surface (i.e., outgoing distribution is a linear functional of the incoming distribution). Particle number conservation requires

$$\int d\mathbf{v}_1\,P(\mathbf{v}_1,\mathbf{v}')=\Theta(-\hat{\mathbf{n}}\cdot\mathbf{v}'). \tag{A4}$$

As an illustration, the form of $K(\mathbf{v},\mathbf{v}_1)$ for elastic specular collisions with a wall at rest is

$$K_s(\mathbf{v}_1,\mathbf{v}')=\delta(\mathbf{v}_1-\mathbf{v}'+2(\hat{\mathbf{n}}\cdot\mathbf{v}')\hat{\mathbf{n}}). \tag{A5}$$

The surface domain Ξ is time dependent, representing vertical oscillations. This can be handled using a sawtooth form for the driving, such that every particle encounters the wall moving into the system at velocity $\mathbf{v}_w=v_w\hat{\mathbf{n}}$. Assume the amplitude of the vibration is small, so that the displacement of the wall can be neglected. Then, it is reasonable to choose specular collisions in the local Galillean frame for which the wall is at rest:

$$P(\mathbf{v}_1,\mathbf{v}')=\Theta(\hat{\mathbf{n}}\cdot(\mathbf{v}_1-\mathbf{v}_w))K(\mathbf{v}_1,\mathbf{v}')\Theta(-\hat{\mathbf{n}}\cdot(\mathbf{v}'-\mathbf{v}_w)), \tag{A6}$$

$$K_s(\mathbf{v}_1,\mathbf{v}')=\delta(\mathbf{v}_1-\mathbf{v}'+2(\hat{\mathbf{n}}\cdot(\mathbf{v}'-\mathbf{v}_w))\hat{\mathbf{n}}). \tag{A7}$$

The wall collision operator becomes

$$T_{Wi}f_i^{(1)}(\mathbf{r},\mathbf{v}_1;t)=\int_\Xi d\mathbf{s}\,\delta(\mathbf{r}-\mathbf{s})\left\{\Theta(\hat{\mathbf{n}}\cdot(\mathbf{v}_1-\mathbf{v}_w))\int d\mathbf{v}'\,\delta(\mathbf{v}_1-\mathbf{v}'+2\hat{\mathbf{n}}\cdot(\mathbf{v}'-\mathbf{v}_w)\hat{\mathbf{n}})\Theta(-\hat{\mathbf{n}}\cdot(\mathbf{v}'-\mathbf{v}_w)) \times|\hat{\mathbf{n}}\cdot(\mathbf{v}'-\mathbf{v}_w)|f_i^{(1)}(\mathbf{r},\mathbf{v}';t)-\Theta(-\hat{\mathbf{n}}\cdot(\mathbf{v}_1-\mathbf{v}_w))|\hat{\mathbf{n}}\cdot(\mathbf{v}_1-\mathbf{v}_w)|f_i^{(1)}(\mathbf{r},\mathbf{v}_1;t)\right\}. \tag{A8}$$

The change in the kinetic energy due to the boundary conditions is

$$\int d\mathbf{r}\int d\mathbf{v}_1\frac{1}{2}m_iv_1^2T_{Wi}f_i^{(1)}(\mathbf{r},\mathbf{v}_1;t) =\int_\Xi d\mathbf{s}\int d\mathbf{v}_1[e_i'(v_1)-e_i(v_1)]|\hat{\mathbf{n}}\cdot(\mathbf{v}_1-\mathbf{v}_w)|\Theta(-\hat{\mathbf{n}}\cdot(\mathbf{v}_1-\mathbf{v}_w))f_i^{(1)}(\mathbf{s},\mathbf{v}_1;t), \tag{A9}$$

where $e_i(v_1)$ and $e_i'(v_1)$ are the kinetic energies for particles coming into and leaving the surface. They are given by

$$e_i(v_1)=\frac{1}{2}m_iv_1^2, \tag{A10}$$

$$e_i'(v_1)=\int d\mathbf{v}\,\Theta(\hat{\mathbf{n}}\cdot(\mathbf{v}-\mathbf{v}_w))\frac{1}{2}m_i v^2\delta(\mathbf{v}-\mathbf{v}_1+2\hat{\mathbf{n}}\cdot(\mathbf{v}_1-\mathbf{v}_w)\hat{\mathbf{n}}) \tag{A11}$$

$$=\frac{1}{2}m_i(\mathbf{v}_1-2(\hat{\mathbf{n}}\cdot\mathbf{v}_1-v_w)\hat{\mathbf{n}})^2\Theta(-\hat{\mathbf{n}}\cdot(\mathbf{v}_1-\mathbf{v}_w)). \tag{A12}$$

Thus, one gets

$$e_i'(v_1)-e_i(v_1)=2m_i v_w^2\left(1-\frac{\hat{\mathbf{n}}\cdot\mathbf{v}_1}{v_w}\right). \tag{A13}$$

Here, v_w is the speed of the wall, taken along the normal $\hat{\mathbf{n}}$. The rate of energy change due to the wall becomes

$$\int d\mathbf{r}\int d\mathbf{v}_1\frac{1}{2}m_i v_1^2 T_{Wi}\,f_i^{(1)}(\mathbf{r},\mathbf{v}_1;t)$$
$$=2m_i v_w^3\int d\mathbf{v}_1\left(1-\frac{\hat{\mathbf{n}}\cdot\mathbf{v}_1}{v_w}\right)^2$$
$$\times\int_{\Xi}d\mathbf{s}\Theta(-\hat{\mathbf{n}}\cdot(\mathbf{v}_1-\mathbf{v}_w))f_i^{(1)}(\mathbf{s},\mathbf{v}_1;t). \tag{A14}$$

If the wall speed is much larger than other characteristic velocities $1-\hat{\mathbf{n}}\cdot\mathbf{v}/v_w\to 1$, and so Eq. (A14) becomes approximately

$$\int d\mathbf{r}\int d\mathbf{v}_1\frac{1}{2}m_i v_1^2 T_{Wi}\,f_i^{(1)}(\mathbf{r},\mathbf{v}_1;t)\to m_i v_w^3 n_i A, \tag{A15}$$

where A is the area of the wall and n_i is the density of incident particles of species i. The rate of change of the temperature is then

$$\frac{\partial T_i}{\partial t}=\frac{2A}{3V}m_i v_w^3-\zeta_i T_i, \tag{A16}$$

which gives the steady state condition (24).

Another estimate is given by representing the incident distribution as a Gaussian

$$2n_i A m_i v_w^3\frac{1}{\sqrt{\pi}}\int_{-\infty}^{v_w/v_{0i}}dv_x^*\left(1-\frac{v_{1i}}{v_w}v_x^*\right)^2 e^{-(v^*+v_2^*)^2}$$
$$=2n_i A m_i v_w v_{1i}^2\left(\frac{1}{2\sqrt{\pi}}(v_w^*+v_2^*)e^{-(v_w^*+v_2^*)^2}+\frac{1}{2}[(v_w^*+v_2^*)^2+2](\mathrm{erf}(v_w^*-v_2^*)+1)\right). \tag{A17}$$

Here $v_w^*=v_w/v_{1i}$, $v_{1i}^2=2T_{1i}/m_i$ characterizes the temperature of the incident particles, and $v_2=v_2^*v_{1i}$ characterizes their mean speed toward the wall. For large $v_w^*+v_2^*$ the condition (A16) is recovered, while for small $v_w^*+v_2^*$ it becomes

$$\frac{\partial T_i}{\partial t}=\frac{4A}{3V}v_w T_{1i}-\zeta_i T_i. \tag{A18}$$

If $T_{1i}\approx T_i$ then the steady state condition for the HCS, constant cooling rate, is recovered.

[1] A. Goldshtein and M. Shapiro, J. Fluid Mech. **282**, 75 (1995); T.P.C. van Noije and M.H. Ernst, Granular Matter **1**, 57 (1998).
[2] J.J. Brey, M.J. Ruiz-Montero, and D. Cubero, Phys. Rev. E **54**, 3664 (1997).
[3] M. Huthman, J. Orza, and R. Brito, Granular Matter **2**, 189 (2000).
[4] V. Garzó and J.W. Dufty, Phys. Rev. E **60**, 5706 (1999).
[5] J.M. Montanero and V. Garzó, Granular Matter **4**, 17 (2002).
[6] A. Santos and J. Dufty, Phys. Rev. Lett. **86**, 4823 (2001); Phys. Rev. E **64**, 051305 (2001).
[7] J.F. Lutsko, Phys. Rev. E **63**, 061211 (2001);
[8] J.W. Dufty, J.J. Brey, and J. Lutsko, Phys. Rev. E **65**, 051303 (2002); J. Lutsko, J.J. Brey, and J.W. Dufty, *ibid.* **65**, 051304 (2002).
[9] A. Barrat and E. Trizac, Granular Matter **4**, 57 (2002).
[10] K. Feitosa and N. Menon, Phys. Rev. Lett. **88**, 198301 (2002).
[11] R. Wildman and D. Parker, Phys. Rev. Lett. **88**, 064301 (2002).
[12] A. Karion and M.L. Hunt, Powder Technol. **109**, 145 (2000).
[13] R. Clelland and C. Hrenya, Phys. Rev. E **65**, 031301 (2002).
[14] J.J. Brey, J.W. Dufty, and A. Santos, J. Stat. Phys. **87**, 1051 (1997).

[15] J.W. Dufty and V. Garzó, J. Stat. Phys. **105**, 723 (2001).
[16] E.W. Grundke and D. Henderson, Mol. Phys. **24**, 269 (1972); L.L. Lee and D. Levesque, *ibid.* **26**, 1351 (1973).
[17] See for instance, D.H.L. Yan, K.Y. Chan, and D. Henderson, Mol. Phys. **88**, 1237 (1996); D.V. Matyushov and B.M. Landanyi, J. Chem. Phys. **107**, 5815 (1997); D. Cao, K.Y. Chan, D. Henderson, and W. Wang, Mol. Phys. **98**, 619 (2000); A. Santos, S.B. Yuste, and M. López de Haro, J. Chem. Phys. **117**, 5785 (2002).
[18] U. Marini, Bettolo Marconi, and A. Puglisi, Phys. Rev. E **65**, 051305 (2002).
[19] Haff's law is a necessary, but not sufficient, condition for the scaling of the HCS. In principle there could be a locally inhomogeneous state such that the total energy is the sum of the thermal energy plus the kinetic energy of convective flows. It is possible that both contributions could decay with the same power law as in Haff's law, but with a different cooling rate ζ. In fact, there is some indication that this may occur in the late stages of instability for the HCS (J. Wakou, R. Brito, and M.H. Ernst, e-print cond-mat/0103086). We assume that in our case the initial state is always HCS and that a transition interval would be seen in any possible evolution to a different Haff's law. The onset of this transition interval is what has been identified here as the violation of Haff's law.
[20] T.P.C. van Noije and M.H. Ernst, Granular Matter **1**, 57 (1998).
[21] D.J. Evans and G.P. Morriss, *Statistical Mechanics of Nonequilibrium Liquids* (Academic Press, London, 1990).
[22] D. Williams and F. MacKintosh, Phys. Rev. E **54**, R9 (1996).
[23] C. Henrique, G. Batrouni, and D. Bideau, Phys. Rev. E **63**, 011304 (2000).
[24] J.J. Brey, M. Ruiz-Montero, and F. Moreno, Phys. Rev. E **62**, 5339 (2000).
[25] V. Garzó and J.W. Dufty, Phys. Fluids **14**, 1476 (2002).
[26] J.R. Dorfman and H. van Beijeren, in *Statistical Mechanics*, edited by B. Berne (Plenum, New York, 1977), Pt. B.